



**QUEEN'S
UNIVERSITY
BELFAST**

Direct D-atom incorporation in radicals: an overlooked pathway for Deuterium Fractionation

Dias, N., Gurusinghe, R. M., Broderick, B. M., Millar, T. J., & Suits, A. G. (2023). Direct D-atom incorporation in radicals: an overlooked pathway for Deuterium Fractionation. *The Astrophysical Journal*, 944(1), Article 77. <https://doi.org/10.3847/1538-4357/acac1d>

Published in:
The Astrophysical Journal

Document Version:
Publisher's PDF, also known as Version of record

Queen's University Belfast - Research Portal:
[Link to publication record in Queen's University Belfast Research Portal](#)

Publisher rights

© 2023 The Authors.

This is an open access article published under a Creative Commons Attribution License (<https://creativecommons.org/licenses/by/4.0/>), which permits unrestricted use, distribution and reproduction in any medium, provided the author and source are cited.

General rights

Copyright for the publications made accessible via the Queen's University Belfast Research Portal is retained by the author(s) and / or other copyright owners and it is a condition of accessing these publications that users recognise and abide by the legal requirements associated with these rights.

Take down policy



The Research Portal is Queen's institutional repository that provides access to Queen's research output. Every effort has been made to ensure that content in the Research Portal does not infringe any person's rights, or applicable UK laws. If you discover content in the Research Portal that you believe breaches copyright or violates any law, please contact openaccess@qub.ac.uk.

Open Access

This research has been made openly available by Queen's academics and its Open Research team. We would love to hear how access to this research benefits you. – Share your feedback with us: <http://go.qub.ac.uk/oa-feedback>



Direct D-atom Incorporation in Radicals: An Overlooked Pathway for Deuterium Fractionation

Nureshan Dias¹, Ranil M. Gurusinghe¹, Bernadette M. Broderick¹, Tom J Millar² , and Arthur G. Suits¹ 

¹Department of Chemistry, University of Missouri, Columbia MO 65211, USA; suitsa@missouri.edu

²School of Mathematics and Physics, Queen's University Belfast, University Road, Belfast BT7 1NN, UK; Tom.Millar@qub.ac.uk

Received 2022 June 24; revised 2022 November 12; accepted 2022 December 13; published 2023 February 14

Abstract

Direct D-H exchange in radicals is investigated in a quasi-uniform flow employing chirped-pulse millimeter-wave spectroscopy. Inspired by the H-atom catalyzed isomerization of C₃H₂ reported in our previous study, D-atom reactions with the propargyl (C₃H₃) radical and its photoproducts were investigated. We observed very efficient D-atom enrichment in the photoproducts through an analogous process of D addition/H elimination to C₃H₂ isomers occurring at 40 K or below. Cyclic C₃HD is the only deuterated isomer observed, consistent with the expected addition/elimination yielding the lowest energy product. The other expected addition/elimination product, deuterated propargyl, is not directly detected, although its presence is inferred by the observations in the latter part of the flow. There, in the high-density region of the flow, we observed both isotopomers of singly deuterated propyne attributed to stabilization of the H+C₃H₂D or D+C₃H₃ adducts. The implications of these observations for the deuterium fractionation of hydrocarbon radicals in astrochemical environments is discussed with the support of a monodeuterated chemical kinetic model.

Unified Astronomy Thesaurus concepts: [Astrochemistry \(75\)](#); [Chemical abundances \(224\)](#); [Isotopic abundances \(867\)](#)

1. Introduction

One of the fascinating observational results in astrochemistry has been the detection of deuterated molecules in high abundance. Many singly, doubly, and even a few triply deuterated molecules have been identified hitherto in various astronomical environments (Tin e et al. 2000; Turner 2001; Lis et al. 2002; Parise et al. 2002, 2004; Roueff & Gerin 2003; Van der Tak et al. 2002; Vastel et al. 2003; Ag undez et al. 2021b). Astonishingly, the observational evidence of the abundance ratios of these deuterated species relative to their fully hydrogenated forms are several orders of magnitude larger than expected based on the cosmic D/H ratio, 2×10^{-5} , set by big bang nucleosynthesis. For example, the abundance ratio of ND₃/NH₃ is around 10^{-3} – 10^{-4} in dark clouds, whereas the statistical value (D/H)³ is roughly 3×10^{-15} , implying a 10^{11} – 10^{12} enhancement (Roueff et al. 2005). This is deuterium enrichment and occurs through a process called fractionation. The reactions that produce deuterium-enriched molecules in this process must selectively increase the deuterium content of product species. Deuterium forms slightly stronger bonds than hydrogen owing to small zero-point energy differences, and this can have a significant impact at low temperature. The effect of this on the reactive species in cold molecular clouds ensures that the deuterium is preferentially bonded into molecules.

Observation of deuterated molecules has also been used to probe various physical parameters such as temperature, ionization fraction, thermal history, and chemistry of astrophysical environments (Roberts & Millar 2000, 2007; Caselli et al. 2002a, 2002b; Amano 2006; Chen et al. 2010; Miettinen et al. 2011; Br unken et al. 2014). However, the usefulness of

deuterated molecules as a probe depends on our ability to understand the dynamics and kinetics of processes by which deuterium is incorporated into them. Considerable effort has thus been devoted to understanding deuterium fractionation in astronomical environments (Willacy & Millar 1998; Roberts & Millar 2000; Roberts et al. 2002; Roueff & Gerin 2003; Albertsson et al. 2013; Ceccarelli et al. 2014). According to the current understanding, the formation of deuterated molecules in the gas phase is dominated by fast ion-neutral reactions (Solomon & Woolf 1973; Watson 1977; Dalgarno & Lepp 1984; Herbst 2003). Abundant molecular ions such as H₃⁺, CH₃⁺, and C₂H₂⁺ undergo exchange reactions with HD, the reservoir for deuterium in dark clouds, to form deuterated ions H₂D⁺, CH₂D⁺, and C₂HD⁺ (Roberts & Millar 2000). These exchange reactions are exothermic and favor the products as the D-bearing ions are more tightly bound due to their reduced zero-point energy. These ions can then transfer a deuterium to simple molecules such as N₂, CO, and atomic oxygen to form simple deuterated molecular ions such as N₂D⁺, DCO⁺, and OD⁺ and initiate the processes leading to deuterium fractionation in many molecules in dark clouds.

The physical environment in cold dark clouds plays a major role in deuterium fractionation. In cold dense regions, where the central temperature of the cloud is 10 K or lower, abundant species that react with H₂D⁺, such as CO, N₂, and O, are depleted by accretion onto the dust grains (Walmsley & Flower 2004), with large enhancements of deuterated species observed in sources with CO depletion (Bacmann et al. 2003; Puananova et al. 2016). Due to this depletion, the enrichment of H₂D⁺ is more pronounced (Roberts & Millar 2000) since, under these conditions, H₂D⁺ can further react with HD to form the other isotopologues of H₃⁺ (Roberts et al. 2003; Caselli et al. 2019). The detailed deuterium fractionation reactions from these isotopologues are described in studies by Roberts et al. and Flower et al. (Roberts et al. 2003; Flower & Walmsley 2004; Walmsley & Flower 2004). In addition to gas-

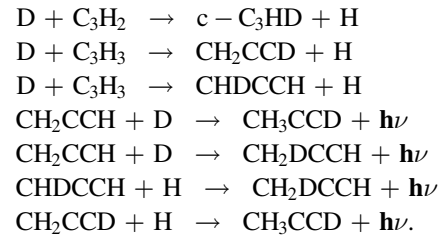
phase deuteration from H_3^+ isotopologues, grain-surface chemistry is also important in deuterium fractionation (Caselli et al. 2002a; Parise et al. 2006). Multiply deuterated species and some of the fully deuterated species are believed to form via surface reactions on dust grains (Brown & Millar 1989a). However, for some deuterated species, the observations largely exceed the predictions and cannot be explained by these models.

In addition to these ion-molecule fractionation and surface reactions, there are very few neutral-atom reactions considered in the literature to form D-bearing molecules. One such significant pathway that involves neutral reactants is formation of OD in dark clouds. Croswell and Dalgarno were the first to predict the possibility of such reactions (Croswell & Dalgarno 1985). According to their predictions, the exchange reaction, $\text{D} + \text{OH} \rightleftharpoons \text{OD} + \text{H}$, yields a large fractionation for OD in dark clouds. The kinetics of this exchange reaction was studied at room temperature and found to have a forward rate coefficient of $1.3 \times 10^{-10} \text{ cm}^3 \text{ s}^{-1}$ (Margitan et al. 1975). Croswell and Dalgarno adopted the same rate coefficient in their prediction and, given that the reaction is exothermic by 810 K, the reverse reaction is unimportant at low temperatures. They predicted OD/OH ratios to be around 0.01 or larger in dark clouds. Subsequently, Brown and Millar predicted that the OD/OH ratio can be large as unity in the clouds under freeze-out conditions (Brown & Millar 1989b). In these regions D_3^+ can form from through the successive reactions of H_3^+ with HD as discussed above. Under these extreme conditions, D_3^+ can be more abundant than H_3^+ and the atomic D/H ratio can also be larger than unity in both gas phase and the grain surface resulting in enhanced OD fractionation. OD was first detected outside of the solar system in the cold low-mass protostar IRAS 16293–2422 using SOFIA, the Stratospheric Observatory for Infrared Astronomy. However, because OH was not observed with SOFIA at infrared wavelengths, an OD/OH ratio was not determined. Although observations at centimeter wavelengths can detect OH, they cannot be used to derive an accurate ratio since they sample an entirely distinct gas with a different density. Nevertheless, a very large fractionation for OD (OD/HDO ≈ 17 –90) was inferred indirectly by Parise et al. (2012) comparing it with HDO in the same source.

Both $c\text{-C}_3\text{H}_2$ and H_2CCC have been observed in dark cloud sources, including TMC-1, with a considerable abundance (Cox et al. 1989; Kawaguchi et al. 1991). The third isomer, HCCCH, is expected to be found in dark clouds but has yet to be discovered due to its negligible dipole moment. The formation pathway for $c\text{-C}_3\text{HD}$ in dark clouds has been studied by several groups and, according to their work, $c\text{-C}_3\text{HD}$ is primarily formed at low temperatures through the initiating reaction of $c\text{-C}_3\text{H}_2$ with H_2D^+ (Gerin et al. 1987; Bell et al. 1988; Spezzano et al. 2016). In extreme conditions, deuteration can also occur with HD_2^+ and D_3^+ , forming the ionic intermediate $\text{C}_3\text{H}_2\text{D}^+$, followed by a dissociative recombination with electrons. In this paper, we demonstrate experimentally for the first time the formation of $c\text{-C}_3\text{HD}$ from direct D-atom-transfer reactions to the C_3H_2 radicals, and suggest this pathway may be of quite general application to the deuteration of hydrocarbon radicals and their subsequent reaction products in interstellar clouds.

In the present study, we apply broadband rotational spectroscopy in a low-temperature flow (Chirped pulse/Uniform Flow, or CPUF) to show efficient D-atom substitution for

H atoms in C_3H_2 isomers and in propargyl radicals as well as H/D addition reactions to $\text{C}_3\text{H}_2\text{D}$ and C_3H_3 . Although these latter addition reactions required collisional stabilization in our experiments to yield the detected products, we indicate them as radiative-association (RA) reactions because it is the primary pathway for the formation of adducts in low-density dark clouds. These reactions are summarized below:



We combine this with astrochemical modeling of various environments to explore the consequences for deuterium fractionation in these clouds. We argue that these pathways may be important in many other systems and contribute to deuterium fractionation under conditions where ionic pathways may be less important.

Previously, we have studied the photodissociation of the propargyl radical and quantified the product branching fractions for various C_3H_2 isomers at low temperature using CPUF in a quasi-uniform flow (Broderick et al. 2018). In that study, we observed H-atom-catalyzed isomerization of C_3H_2 isomers to yield the more stable $c\text{-C}_3\text{H}_2$ isomer. The $c\text{-C}_3\text{HD}$ form has been observed in many sources with fractionation ratios ranging from 0.08 to 0.23 (Chantzos et al. 2018), but current models underestimate its observed fractional abundance (Markwick et al. 2001; Chantzos et al. 2018). This discrepancy, along with the results of our previous study, motivated us to incorporate D atoms to our experimental studies. Here, we report direct D-atom incorporation to the C_3H_2 isomers in an analogous process. Following the recent discovery of propargyl radical in Taurus Molecular Cloud 1 (TMC-1), we suggest deuterated propargyl radicals will likely be abundant interstellar molecules (Agúndez et al. 2021a), although their detection is hampered by the small dipole moment of propargyl.

The deuterated isotopomer of propyne, CH_2DCCH , was first detected in TMC-1 by Gerin et al. (1992). About a decade later the other isotopomer, CH_3CCD , was detected in TMC-1 by Markwick et al. (2005). The main formation of these species involves ion-neutral reactions. In the present study, we propose a possible pathway for the formation of deuterated propyne (CH_2DCCH and CH_3CCD) in the interstellar medium by radiative association involving propargyl or its deuterated isotopologues. Based on the recent discovery of doubly deuterated propyne in L483 (Agúndez et al. 2021b), we argue below that it can also be produced through radiative-association reactions. Although experimentally we observe the products of these reactions, and the decay of some species, at this stage, we cannot calibrate the densities as would be needed to measure the rates. Nevertheless, the experimental observations suggest the picture we outline, and the modeling we show provides confirmation of the potential impact. Concurrent with the experiments we performed astrochemical modeling using the UDfA Rate 13 code and the results of the simulations are compared with observations from the literature.

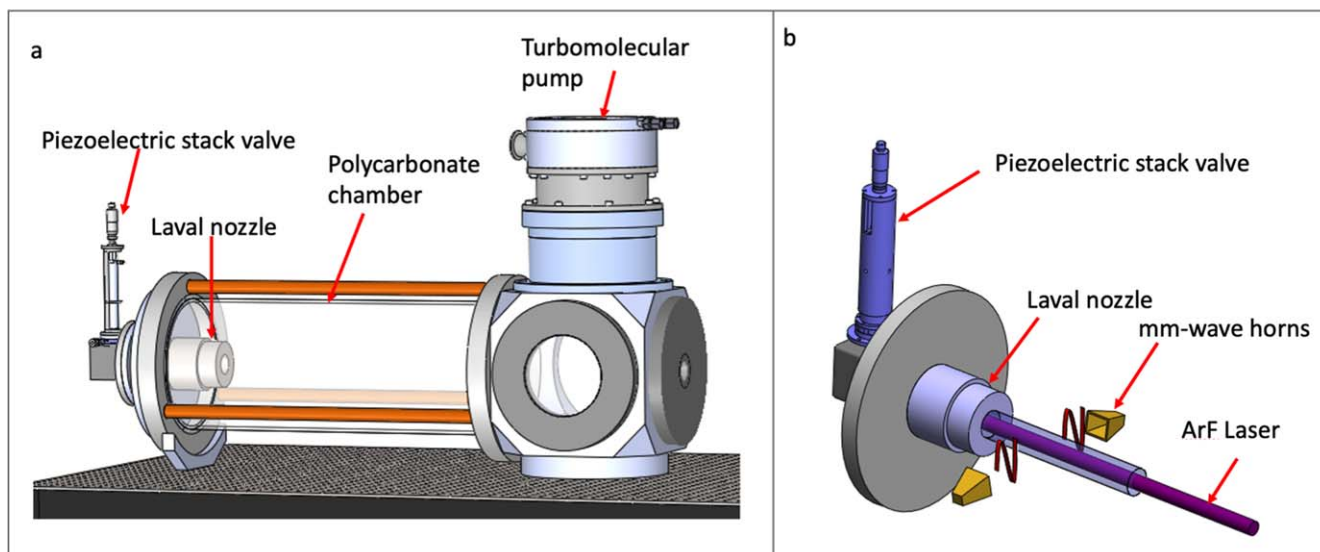


Figure 1. (a) Chirped-pulse experimental apparatus. (b) Schematic of the experimental setup. To generate the He quasi-uniform flow, a piezoelectric stack valve generates a high throughput gas pulse, which is expanded through the Laval nozzle. The reaction is initiated by the ArF laser, which propagates counter to the flow. The products are detected by broadband rotational spectroscopy.

2. Experimental Description

The experiments are performed in our CPUF experimental setup described previously (Abeysekera et al. 2014; Oldham et al. 2014; Park & Field 2016). It comprises a pulsed Laval flow coupled to a chirped-pulse millimeter-wave spectrometer. The CPUF experimental apparatus and the schematic of the experimental setup is depicted in Figures 1(a) and (b). Here we use a “quasi-uniform” Laval flow in which the initial conditions are uniform and high density within the nozzle, which is followed by a second expansion to a low-density and low-temperature detection region that is optimized for the millimeter-wave signal (Broderick et al. 2018; Dias et al. 2018). The number density of the uniform region is approximately a few 10^{16} molecules cm^{-3} and this persists for several centimeters. The density declines by several orders of magnitude in the detection region preventing the collisional attenuation of the millimeter-wave signal. The characteristics of the quasi-uniform flow are described in depth in our earlier publication (Broderick et al. 2018) and the details of current millimeter-wave circuitry are outlined in our previous publications (Abeysekera et al. 2015; Gurusinghe et al. 2021a; Dias et al. 2022).

In this experiment, the flow consists of 1% of propargyl bromide (98% purity Sigma Aldrich; seeded in He) and 1% of ND_3 (99% purity Sigma Aldrich; seeded in He) for generation of radicals and D atoms. After the flow is established, 20 mJ of a loosely focused 193 nm laser radiation fires 10 μs before the first millimeter-wave pulse. Given the area of the laser beam, this corresponds to a fluence of 6×10^{16} photons cm^{-2} per pulse. A single photon dissociates the propargyl bromide and ND_3 resulting mostly in propargyl (C_3H_3), ND_2 , D atoms, and H atoms (Nakajima et al. 1991; Lee & Lin 1998; Foley et al. 2019). The C_3H_3 can react with ND_2 to give a range of products; these are the subject of a separate study reported elsewhere (Gurusinghe et al. 2021b). A second photon of the same wavelength that is absorbed within the 20 ns laser pulse may dissociate the propargyl radical giving mainly C_3H_2 isomers and H atoms. For each gas pulse, the rotational spectra are collected at 5 μs intervals up to 175 μs using the fast frame

capabilities of the oscilloscope. This permits us to investigate the detailed dynamics of the reactions within the flow on this timescale.

Broadband scans were used initially to identify the rotational lines corresponding to the products of photodissociation and reaction in the 70–92 GHz region. Upon identifying the lines, resonant frequency $\pi/2$ pulses of varying durations were used to excite the individual rotational lines observed in the initial broad chirps. The millimeter-wave transition frequencies and the line strength values are extracted from the Cologne Database for Molecular Spectroscopy (CDMS) and summarized in Table A1 in the Appendix. Both up and down chirps were used to acquire and average the spectra to compensate for the dephasing effects. The rotational spectra corresponding to the photoproducts of propargyl radical dissociation and the products arising from the D-atom reactions with radicals were obtained. The time evolution of the integrated intensities are then obtained from the corresponding rotational lines.

3. Astrochemical Modeling

We have used the UDFa Rate 13 codes (from now on Rate 13 code, available at www.udfa.net), with an updated, deuterated version of the UDFa Rate 12 network to investigate the impact of inclusion of D-atom reactions on the abundance and fractionation of $c\text{-C}_3\text{HD}$ and other related species in our study (McElroy et al. 2013). The updated version of the reaction network now includes 846 species with 24,952 reactions. New reactions involving propargyl, propyne, and their deuterated analogues were added to this rate file and are given in Table A2 in the Appendix with their collisional rate constants and energy barriers. We used standard physical conditions for a cold, dark molecular cloud, similar to those often adopted for TMC-1, and for a warmer, denser cloud, similar to those in Orion Molecular Cloud (OMC) ridge. For TMC-1, we adopted a typical gas temperature of $T_g = 10$ K and density of $4 \times 10^4 \text{ cm}^{-3}$ (Cernicharo et al. 2021) and, for OMC, we use a gas temperature of 70 K and a slightly higher density, $1 \times 10^5 \text{ cm}^{-3}$ (Sutton et al. 1995; Tercero et al. 2011), although the latter gives 60 K for T_g . We also used freeze-on

conditions to predict the fractional abundances in TMC-1 and chose the same density of $4 \times 10^4 \text{ cm}^{-3}$ for these conditions. For both TMC-1 and OMC, we used a standard cosmic ray ionization rate of $1.3 \times 10^{-17} \text{ s}^{-1}$. Relative to the total hydrogen nucleon density, we adopted initial fractional abundances of 1.5×10^{-5} for HD, which is similar to its cosmic abundance, and, for atomic D, we used 3×10^{-10} . We took initial elemental abundances from McElroy et al. (2013) but reduced their initial O abundance from 3.2×10^{-4} to 1.3×10^{-4} corresponding to a carbon-rich environment. Loomis et al. (2021) reported that a C/O ratio of 1.1, similar to our value, gives the best fits for the observed species HC₁₁N in TMC-1. An initially low C/O ratio leads to a relatively low abundances of long carbo-chain and related species (Agúndez & Wakelam 2013; Agúndez et al. 2021a).

We note that these simple one-point models neglect the intrinsic physical complexity of TMC-1 and the OMC region. For example, chemistry in a much more physically detailed model of TMC-1 has been studied recently by Wakelam et al. (2021). Indeed, our models are somewhat simplistic from a chemical modeling perspective since they also neglect the extensive spin-state chemistry involved in the deuteration of H₂ and its related ions, specifically H₂D⁺, HD₂⁺, and D₃⁺, as well as the possibility that fractionation can also take place through grain-surface reactions.

In particular, the efficacy of fractionation via these deuterated ions depends on the ortho-para ratio of H₂ since para-H₂ lies 170.5 K higher in energy and therefore possesses a much lower energy barrier in reactions that destroy its deuterated counterparts. Although radiative transitions between ortho and para forms are forbidden, proton exchange reactions with H⁺ and H₃⁺ are known to reduce the ortho-para ratio with time, from an initial (high-temperature) value of 3 to values around 10^{-3} at long times for a dark cloud similar to TMC-1, with detailed effects indicating a reduction in fractionation over models that neglect spin-state effects (Flower et al. 2006; Majumdar et al. 2016). Nevertheless, we believe that there is some value in presenting these calculations to gain some estimate of the impact of such reactions on the fractionation of hydrocarbon molecules and to motivate future study.

4. Experimental Results

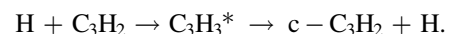
Direct D-atom-exchange reactions were studied in a quasi-uniform Laval flow of helium in which precursor molecules were seeded then exposed to 193 nm laser radiation as described above. In the past, we have used the variation of the density in the quasi-uniform flow to characterize the density-dependent chemistry observed in the experiment, as regions of different conditions arrive at the detector at well-defined times (Broderick et al. 2018; Gurusinghe et al. 2021b). This approach is employed here as well. Rotational spectroscopy in the 70–92 GHz range is used to investigate the products formed as a function of delay between the laser initiation and the probe time (hence origin point in the flow). The results are given in Figure 2, showing six spectral lines corresponding to rotational transitions of the six different products we observed. These correspond to l-C₃H₂, c-C₃H₂, c-C₃HD, CH₃CCH, CH₂DCCCH, and CH₃CCD. The spectra are acquired in 5 μs intervals, and the laser fires between the first and second frame (5 μs after the first millimeter-wave pulse is fired). The lines that appear around 82.5 GHz in all frames are artifacts due to

the millimeter-wave electronics and are independent of the valve and laser.

Figure 3(a) illustrates the time-evolution plot of the total integrated intensities of all the products observed in this study normalized to the transition strength and the rotational partition function. Figure 3(b) depicts the products corresponding to the C₃H₂ isomers resulting from the direct photodissociation of the propargyl radical and the c-C₃HD resulting from its reaction with D atoms. The c-C₃H₂ isomer appears 60 μs after the laser and persists until 120 μs. The l-C₃H₂ isomer appears after 30 μs and vanishes around 80 μs. The initial delay in the appearance of these two products is attributed to the distinct levels of rotational and vibrational cooling that the molecules undergo subsequent to their formation. Notable features in the time-evolution plot are the disappearance of l-C₃H₂, the appearance of c-C₃HD, the sharp rise in c-C₃H₂ at around 75 μs, and the rise in propyne and deuterated propyne signal at around 90 μs. Figure 3(c) shows the time-evolution plot of propyne and its deuterated isotopologues resulting from the reaction of deuterated propargyl with H atoms or normal propargyl with D atoms. These products appear later in the spectra corresponding to the high-density region near the nozzle throat. The propyne products appear 90 μs after the laser and peak at 135 μs. In these spectra, the total integrated intensity for CH₂DCCCH is roughly twice as high as that for CH₃CCD and both species exhibit similar time evolution.

5. Experiments: Discussion

We first discuss the D-H exchange results seen in the experiment. Although, to our knowledge, D-H exchange reactions between C₃H_n ($n = 2, 3$) isomers have never been explored before, the addition/elimination of H atoms to these species has been investigated using both experimental and theoretical methods. Klippenstein et al. (2015) have employed high-level electronic structure methods with classical trajectory calculations to determine the microcanonical rate constants for the dissociation of propargyl radical and the reverse: recombination of C₃H₂ isomers with H atoms under a variety of conditions (Klippenstein et al. 2015). The results of the electronic structure methods, as well as high-pressure rate constants for H-atom addition reactions with C₃H₂ isomers at temperatures ranging from 500 to 2500 K, demonstrate that this recombination is fast and proceeds without a barrier. Our previous experimental study shows that these reactions are also fast at low temperatures (Broderick et al. 2018). In the flow, the propargyl produced by this recombination is much colder than the initial propargyl formed via photodissociation. However, the propargyl formed through this recombination still possesses some energy and requires a third body to stabilize it through collision or it will redissociate. Such stabilization is not possible in our medium-density region. Therefore, it dissociates back to C₃H₂ but now exclusively to c-C₃H₂, the most stable isomer, in a process of H-catalyzed isomerization:



The importance of these H-atom-catalyzed isomerization reactions in Titan’s atmosphere is also discussed by Hébrard et al. (2013).

We note that other species are present in the flow as discussed in our previous work (Broderick et al. 2018; Gurusinghe et al. 2021b) and mentioned above. Aside from deuterium atoms, the primary deuterated species will be ND₂.

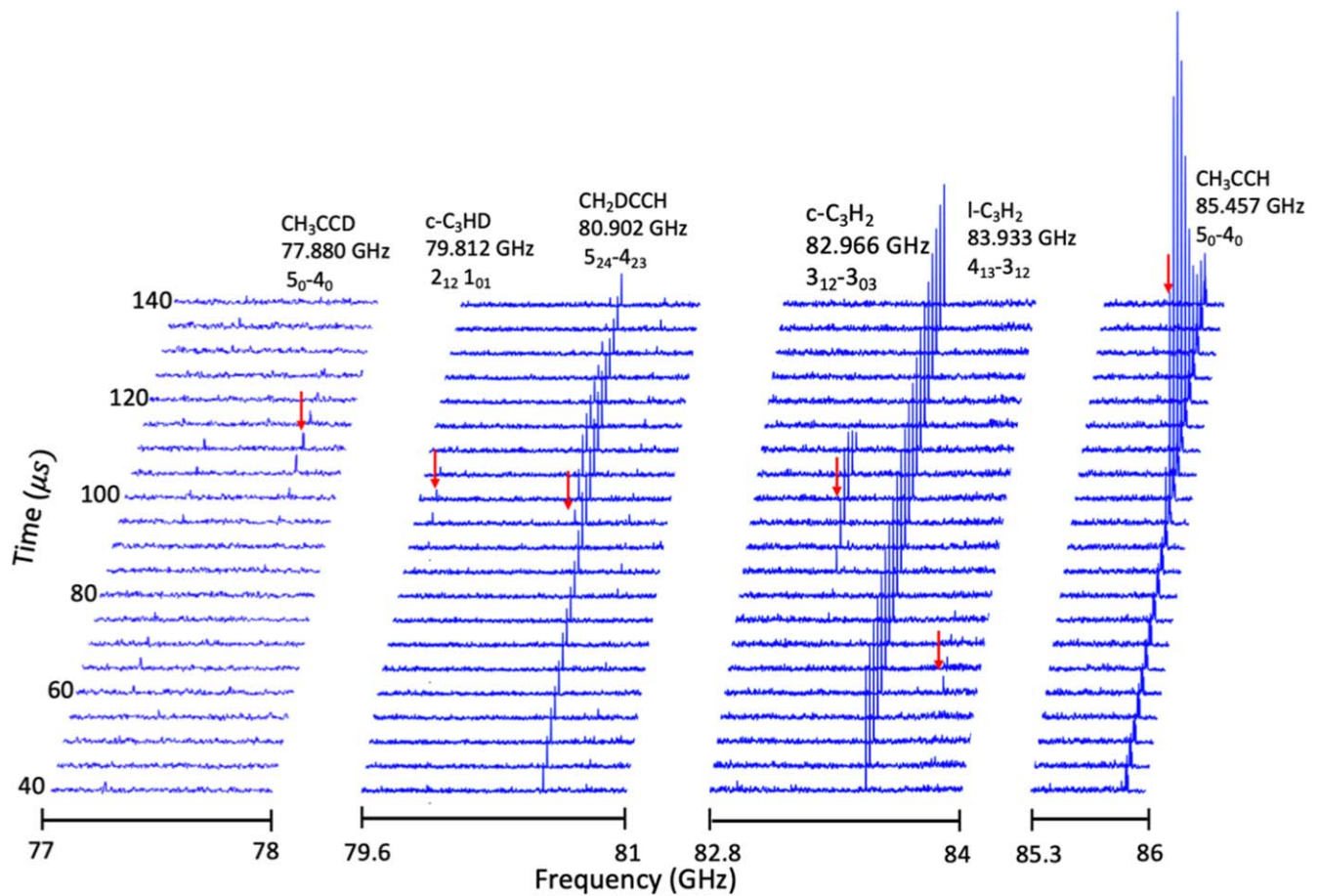


Figure 2. Rotational spectra of the products observed in this experiment. Probe delay after laser pulse is indicated on left. The red arrows indicate the positions of each rotational line observed, and the details of each line are indicated just above it.

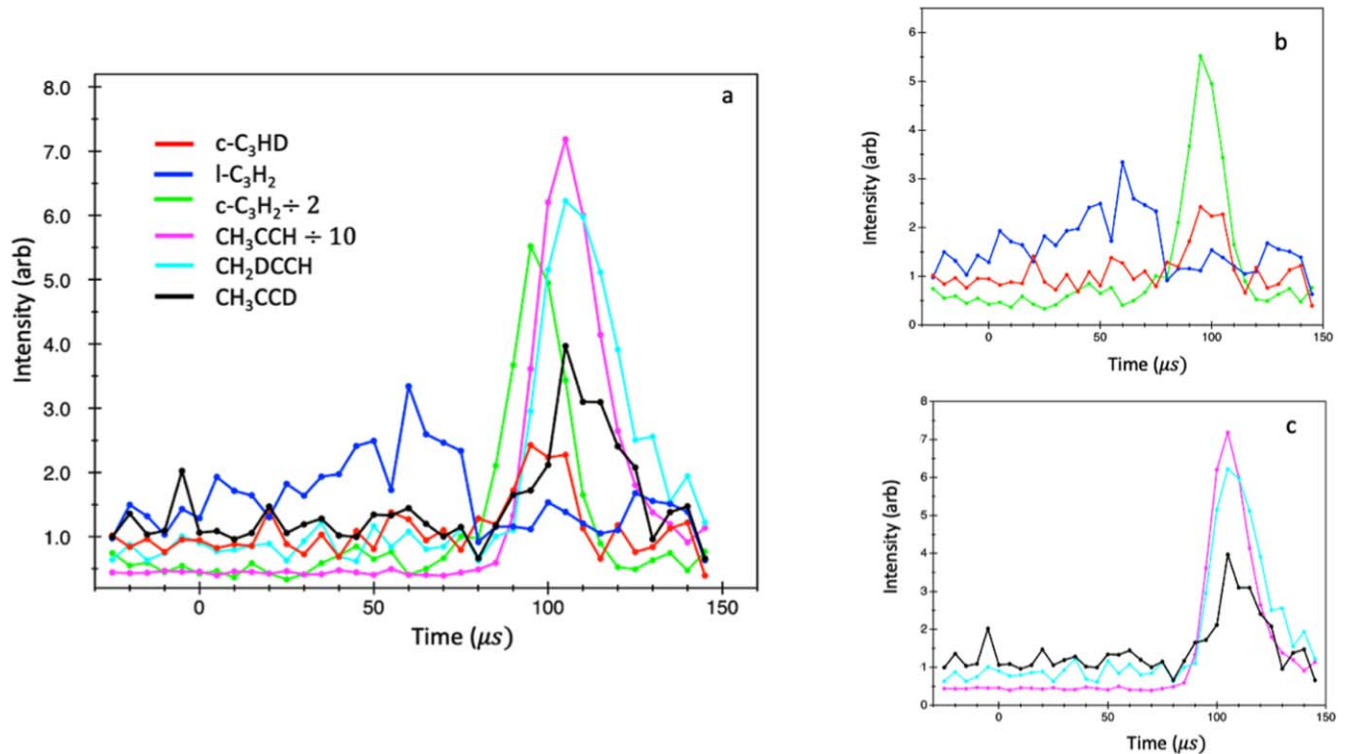


Figure 3. (a) The time-evolution integrated intensities of products observed in the experiment, (b) time-evolution integrated-intensity plot of C_3H_2 species observed, and (c) the time-evolution integrated-intensity plot of propyne species observed in this study.

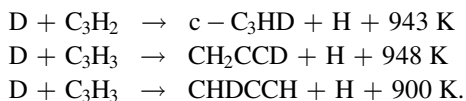
Reaction of ND_2 with C_3H_2 or C_3H_3 to give any of the detected species is endothermic and not likely to contribute to the measured signals under our experimental conditions.

The present study confirms the efficient incorporation of D atoms into C_3H_2 isomers resulting from the reaction of propargyl bromide photoproducts with D atoms, and it thus reveals a new pathway to deuterium fractionation. In a manner analogous to $\text{H}+\text{C}_3\text{H}_2$ recombination, $\text{D}+\text{C}_3\text{H}_2$ recombination is fast and barrierless and mimics the H-atom-catalyzed isomerization. The combination of C_3H_2 with D atoms forms deuterated propargyl, which will dissociate exclusively to $c\text{-C}_3\text{HD}$ in our lower or medium-density region at low temperature. We examined for $l\text{-C}_3\text{HD}$ in and found no lines that corresponded to it in our spectra, confirming that the dissociation was exclusive to $c\text{-C}_3\text{HD}$. We observe the appearance of $c\text{-C}_3\text{HD}$ around $100 \mu\text{s}$ which corresponds to the medium-density region in the flow. In this region, termolecular collisions are negligible, and the products formed in this region cannot be stabilized by collisions.

We also observed propyne and its deuterated isotopologues appearing around $110 \mu\text{s}$, which corresponds to the higher density region where products can be stabilized through third-body collisions. This must result either from H addition to deuterated propargyl radicals, or D addition to normal propargyl radicals, or both. Deuterated propargyl may be formed through D-H exchange just as we describe for $c\text{-C}_3\text{HD}$ formation. However, its small dipole moment precludes monitoring propargyl directly in this study. Harding et al. (2007) have shown H recombination with propargyl is also fast and barrierless. Different reactivities are predicted for the two resonance structures of the propargyl radical (i.e., when the attack occurs on the methylenic or “head” side or the acetylenic “tail” side), but they appear to approach similar rates at low temperature. In any case, scrambling of the H/D location is possible, in particular via cyclic intermediates $c\text{-C}_3\text{H}_2\text{D}$ or $c\text{-C}_3\text{H}_3\text{D}$, for both pathways that may lead to deuterated propyne.

In Figure 3, we see that the intensity for the deuterated propyne isotopomer, CH_2DCCH , is roughly twice that for CH_3CCD , supporting the importance of scrambling en route to formation of deuterated propyne. However, we observed different abundance ratios for CH_2DCCH to CH_3CCD depending on experimental conditions and propargyl radical precursor. In some cases, the intensities of both deuterated propyne isotopomers were nearly identical, whereas in others, CH_3CCD was not detected. The variation in relative yield we observe suggests competition between quenching of the hot propyne or allene adducts versus isomerization and scrambling, with final branching depending strongly on the precise pressure and H and D concentrations. This will be the subject of a future study.

Both reaction pathways identified here are strongly exoergic for D-H exchange:



This contrasts with the ion-neutral reaction that initiates most of the deuterium fractionation as previously understood:

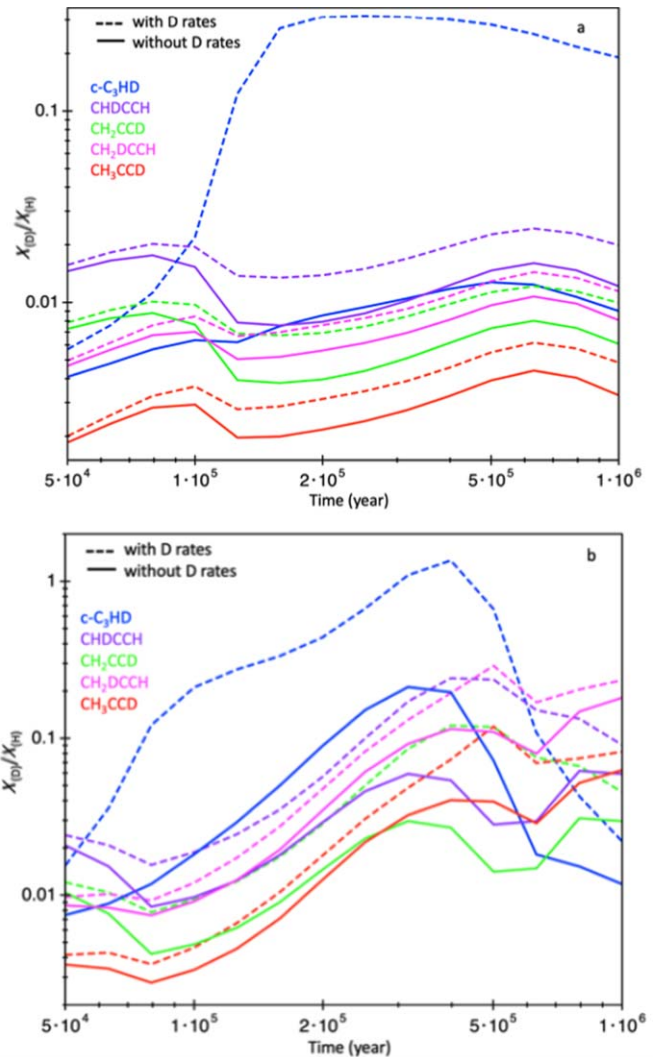
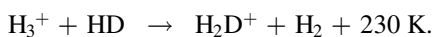


Figure 4. Modeled fractionation ($X_{\text{D}}/X_{\text{H}}$), defined as the ratio of the deuterated to the undeuterated isotopologue, for species of interest in TMC-1 (a) without freeze-out and (b) with freeze-out conditions.

The consequence of this is that deuterium fractionation via the D-H exchange mechanism can contribute at significantly higher temperatures than H_2D^+ as discussed in the modeling below.

6. Astrochemical Modeling Results

6.1. TMC-1

The time evolution of the fractionation, $X_{\text{D}}/X_{\text{H}}$ of $c\text{-C}_3\text{HD}$, CHDCCH , CH_2CCD , CH_2DCCH , and CH_3CCD and was modeled using the Rate 13 code and their abundances are compared for cases with and without the D-H-atom-exchange reactions. These results, in terms of the time evolution of their molecular fractionation ratios, are summarized for TMC-1 in Figure 4(a) with freeze-out conditions off and in 4(b) with freeze-out conditions on. Initial abundances and the conditions used in the modeling are described in the astrochemical modeling section. Figure 4(a) shows that the inclusion of D-exchange reactions to the C_3H_2 isomers significantly increases the fractionation of $c\text{-C}_3\text{HD}$, to a level slightly higher than its observed value in TMC-1 (see Table 1 for a comparison of observed and predicted fractional abundances and fractionation ratios at a time of 1.5×10^5 yr). Moreover, the exchange reaction of D atoms with

Table 1
Observed and Predicted Fractional Abundances and Fractionation Ratios in TMC-1 with Freeze-out Off and Freeze-out On Conditions

				c-C ₃ HD	CHDCCH	CH ₂ CCD	CH ₂ DCCH	CH ₃ CCD
Without freeze-out conditions	1.5×10^5 yr and number density of $50,000 \text{ cm}^{-3}$	Abundance	Observed	1.20E-09 ^a	9.20E-10 ^b	2.00E-10 ^c
			Without D reactions	2.59E-09	3.56E-12	1.78E-12	3.76E-10	1.44E-10
			With D-atom reactions	7.40E-08	6.25E-12	3.12E-12	5.05E-10	2.07E-10
		Fractionation	Observed	0.08–0.16 ^a	0.106 ^b	0.04–0.11 ^c
			Without D reactions	0.007	0.007	0.003	0.005	0.002
			With D-atom reactions	0.271	0.014	0.007	0.007	0.003
With freeze-out conditions	1.5×10^5 yr and number density of $50,000 \text{ cm}^{-3}$	Abundance	Without D reactions	2.35E-09	1.35E-12	6.74E-12	1.96E-10	7.15E-11
			With D-atom reactions	1.24E-08	2.55E-12	1.27E-12	2.74E-10	1.04E-10
			Fractionation	Without D reactions	0.049	0.018	0.009	0.020
		With D-atom reactions	0.334	0.035	0.017	0.028	0.011	

Notes.^a Chantzos et al. (2018).^b Cabezas et al. (2021a).^c Markwick et al. (2005).

Table 2
Main Formation and Destruction Reactions of Species of Interest in TMC-1 at a Model Time of 1.5×10^5 yr

Species	Main Formation Reactions	%	Main Destruction Reactions	%
c-C ₃ HD	$D + C_3H_2 \rightarrow C_3HD + H$	78	$HCO^+ + C_3HD \rightarrow C_3H_2D^+ + CO$	33
	$e^- + C_3H_2D^+ \rightarrow C_3HD + H$	21		
CHDCCH	$D + CH_2CCH \rightarrow CHDCCH + H$	38	$CHDCCH + H \rightarrow CH_2DCCH + PHTN$	38
	$C + C_2H_3D \rightarrow CHDCCH + H$	35		
CH ₂ CCD	$D + CH_2CCH \rightarrow CH_2CCD + H$	38	$CHDCCH + H \rightarrow CH_2CCHD + PHTN$	38
	$C + C_2H_3D \rightarrow CH_2CCD + H$	35		
CH ₂ DCCH	$CH_2CCH + D \rightarrow CH_2DCCH + PHTN$	11	$CH_2CCD + H \rightarrow CH_3CCD + PHTN$	38
	$e^- + C_3H_6D^+ \rightarrow CH_2DCCH + H_2 + H$	33	$CH_2CCD + H \rightarrow CH_2CCHD + PHTN$	38
	$CHDCCH + H \rightarrow CH_2DCCH + PHTN$	51	$CH_2DCCH + CN \rightarrow CH_2DC_3N + H$	22
CH ₃ CCD	$CH_2CCD + H \rightarrow CH_3CCD + PHTN$	47	$CH_2DCCH + CN \rightarrow CH_3C_3N + D$	16
	$e^- + C_3H_6D^+ \rightarrow CH_3CCD + H_2 + H$	27	$CH_2DCCH + C \rightarrow C_4H_2D + H$	27
	$CH_2CCH + D \rightarrow CH_3CCD + PHTN$	10	$CH_3CCD + CN \rightarrow CH_3C_3N + D$	10
			$CH_3CCD + CN \rightarrow CH_2DC_3N + H$	27
			$CH_3CCD + C \rightarrow C_4H_2D + H$	29

Table 3
Observed and Predicted Fractional Abundances and Fractionation Ratios in OMC at a Model Time of 2×10^5 yr

		c-C ₃ HD	CHDCCH	CH ₂ CCD	CH ₂ DCCH	CH ₃ CCD
Abundance	Without D reactions	1.62E-09	1.22E-11	6.11E-12	1.38E-10	5.48E-11
	With D-atom reactions	2.74E-08	2.30E-11	1.15E-11	2.00E-10	8.69E-11
Fractionation	Observed	<0.05 ^a	...
	Without D reactions	0.012	0.024	0.012	0.010	0.004
	With D-atom reactions	0.278	0.047	0.024	0.015	0.006

Note.

^a Millar (1997).

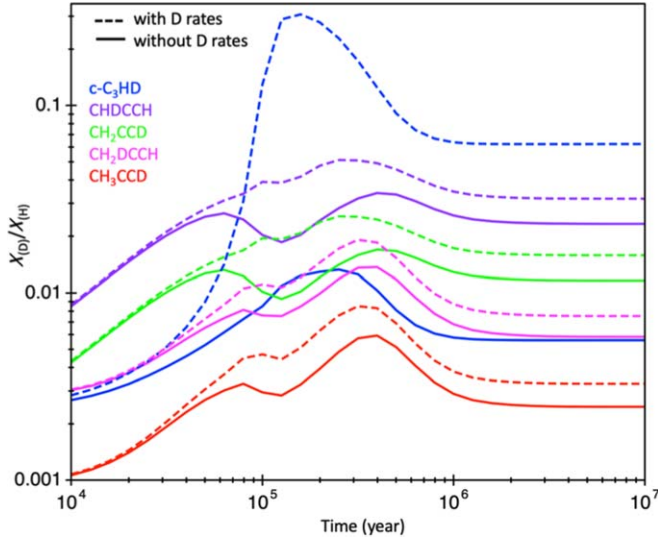


Figure 5. Modeled fractionation of species of interest in Orion Molecular Cloud.

the propargyl radical



also increases the fractionation of deuterated propargyl radicals. The fractionation for deuterated propyne, which forms primarily from the radiative associations of H atoms with CHDCCH and CH₂CCD, increases slightly as the consequence of the increased deuterated propargyl fractionation. Table 2 summarizes the reactions that contribute more than 10% to the formation and destruction of species mentioned above for the freeze-on and freeze-off models. Our analysis shows that the main reactions that lead to the formation of c-C₃HD, and CHDCCH/CH₂CCD are the D-atom-transfer reactions to the C₃H₂ and CH₂CCH radicals, respectively. Figure 4(b) shows the time evolution of the fractionation of related species in TMC-1 when we include the freeze-out conditions. For this, we chose 1.5×10^5 yr as the time when our model most closely reproduces the fractionation results. This condition further increased the fractionation of the above-mentioned species. Under these conditions, the fractionation of c-C₃HD becomes slightly larger than its observed and projected values in the absence of freeze-out conditions. Note that, although the fractionation ratios are large at long times, $\sim 10^6$ yr, the underlying molecular abundances are very small due to freeze-out.

6.2. Orion Ridge Cloud

Figure 5 shows a comparison of the predicted fractionation of species mentioned above in the warmer and denser Orion ridge cloud. At higher temperatures, above 20–25 K, the back reaction of H₂ with H₂D⁺ becomes efficient and deuteration via this ion becomes unimportant. However, at such temperatures, the D-atom incorporation to the radicals is still fast and barrierless and the reverse reaction prohibited. As in the case for TMC-1, when we include the D-atom incorporation to the radicals, the fractionation of all the species mentioned above increased. However, the comparison between predicted and observed fractionations of c-C₃HD and deuterated propargyl is not possible in OMC due to the lack of observational evidence for the presence of both deuterated species. Table 3 compares the observed and predicted fractional abundances and fractionation ratios at a time of 2×10^5 yr. According to our findings, the D-atom-transfer reactions to the C₃H₂ and CH₂CCH radicals are the primary pathway for the production of both c-C₃HD and deuterated propargyl (see Table 4).

7. Astrochemical Modeling Discussion

The principal pathways to deuterium fractionation are well established and believed to occur chiefly through ion-molecule reactions and grain-surface chemistry. However, for some species, the observations vastly exceed what simulations predict. This inconsistency has been observed for many molecules including NH₂D, DCN, N₂D⁺, c-C₃HD, and DC₃N. For some of these species, the modeled fractionation becomes somewhat consistent with the observed value at the steady state. However, many of these dark cloud sources have not yet reached the steady state.

For c-C₃HD, our basic model, without D-atom-exchange reactions and freeze-out, gives $X_{(\text{D})}/X_{(\text{H})} = 0.007$ at 1.5×10^5 yr and 0.015 at steady state, much lower than the range observed in TMC-1, 0.08–0.16. Some of these observational values can be uncertain due to large optical depths or self-absorption in the non-deuterated species. However, c-C₃HD has been observed abundantly in many dark cloud sources, indicating that there are few uncertainties associated with its measurements (Chantzou et al. 2018). Interestingly, in some sources, the fractionation for c-C₃HD becomes comparable or higher than its ostensible deuterated source, H₂D⁺ (0.1) or CH₂D⁺ (0.02). This is an indication that the deuteration of c-C₃HD may not occur exclusively from the commonly expected reactions. Howe and Millar have tested possible alternative routes to the deuterium fractionation (Howe & Millar 1993). Direct deuteration of ionic species by reaction with D atoms or HD was discussed. Fractionation for c-C₃HD

Table 4
Main Formation and Destruction Reactions of Species of Interest in OMC at a Model Time of 2×10^5 yr

Species	Main Formation Reaction	%	Main Destruction Reaction	%
c-C ₃ HD	D+C ₃ H ₂ → C ₃ HD + H e- + C ₃ H ₂ D ⁺ → C ₃ HD + H	69 29	HCO ⁺ + C ₃ HD → C ₃ H ₂ D ⁺ + CO	48
CHDCCH	D + CH ₂ CCH → CHDCCH + H C+C ₂ H ₃ D → CHDCCH + H	46 38	CHDCCH+H → CH ₂ DCCH + PHTN CHDCCH+H → CH ₂ CCHD + PHTN	35 35
CH ₂ CCD	D + CH ₂ CCH → CH ₂ CCD + H C+C ₂ H ₃ D → CH ₂ CCD + H	46 38	CH ₂ CCD + H → CH ₃ CCD + PHTN CH ₂ CCD + H → CH ₂ CCHD + PHTN	35 35
CH ₂ DCCH	CH ₂ CCH + D → CH ₂ DCCH + PHTN e- + C ₃ H ₆ D ⁺ → CH ₂ DCCH + H ₂ + H CHDCCH + H → CH ₂ DCCH + PHTN	11 24 51	CH ₂ DCCH + CN → CH ₂ DC ₃ N+H CH ₂ DCCH + CN → CH ₃ C ₃ N+D	49 16
CH ₃ CCD	CH ₂ CCD + H → CH ₃ CCD + PHTN e- + C ₃ H ₆ D ⁺ → CH ₃ CCD + H ₂ + H CH ₂ CCH + D → CH ₃ CCD + PHTN	59 18 13	CH ₃ CCD + CN → CH ₃ C ₃ N+D CH ₃ CCD + CN → CH ₂ DC ₃ N+H	16 49

improved with the inclusion of the reaction of $C_3H_3^+$ with HD followed by the dissociative recombination. Millar et al. (1989) also noted this discrepancy and suggested that the enhanced ratio may be due to preferential ejection of H atoms from the ionic intermediate during the dissociative recombination (Millar et al. 1989).

Our modeling indicates that more than 78% of $c\text{-}C_3\text{HD}$ is formed through the D-atom exchange involving the C_3H_2 radicals in cold conditions, and in warm conditions such as in the Orion cloud, 69% of $c\text{-}C_3\text{HD}$ is formed through the same reaction (see Table 4). The fractionation ratio increased to 0.27 under TMC-1-like conditions by including D-atom-transfer reactions to the C_3H_2 isomers in the model, comparable to the observed range of 0.08–0.16. The calculated value increases to 0.33 when freeze-out is applied. In warm OMC-like conditions, the fractionation has increased from 0.012 to 0.28 when the D-atom-exchange reaction is included. However, since $c\text{-}C_3\text{HD}$ has not yet been detected in this source, a comparison between theory and observation is not possible at present.

As shown in Figures 4 and 5, our chemical modeling predicts increased abundances for deuterated propargyl when we include D-atom-exchange reactions, increasing from 0.007 to 0.014 for CHDCCH and from 0.003 to 0.007 for CH_2CCD in cold TMC-1-like conditions. In warm conditions, the fractionation increased from 0.024 to 0.047 for CHDCCH and from 0.012 to 0.024 for CH_2CCD . Both our experiments and modeling indicate that deuterated propargyl should be present at an observable level in both TMC-1 and the Orion molecular cloud. Agúndez et al. (2021a) has recently discovered the propargyl radical in TMC-1 using the Yebes 40 m telescope with a fractional abundance relative to H_2 of 8.7×10^{-9} suggesting that the propargyl radical is one of the most abundant radicals ever found in TMC-1 (Agúndez et al. 2021a). This further implies deuterated isotopologues of propargyl should also present in these regions. Searches for these species in TMC-1 are thus urgently required to test the deuteration mechanism discussed herein.

The radiative-association reaction, $H + CH_2CCH \rightarrow CH_3CCH + h\nu$, is included in the KIDA database (Kinetics Database for Astrochemistry) (Wakelam et al. 2012). We have added the corresponding D-atom reactions in our chemical modeling (See Table 1 in Appendix). According to our model, these radiative-association reactions between $D + CH_2CCH/CHDCCH$ are primarily responsible for the generation of deuterated propyne. In cold TMC-1-like conditions, the fractionation increased from 0.005 to 0.007 for CH_2DCCH and from 0.002 to 0.003 for CH_3CCD . However, the fractionation predicted by the model is still significantly lower than the observed fractionation (0.106 for CH_2DCCH and 0.04–0.11 for CH_3CCD). With the introduction of freeze-out conditions, the prediction further increases toward the observed values. Under these conditions the fractionation of CH_2DCCH and CH_3CCD is 0.028 and 0.011, respectively, but much higher at later times ($\approx 5 \times 10^5$ yr). At these times, the fractional abundances are still significantly higher, but lower than the observed values. The plot of fractional abundances of all the species observed in TMC-1 was calculated by incorporating the D-atom reactions and freeze-out conditions, is shown in Figure 1 in the Appendix. In warm (OMC) conditions, the fractionation improved from 0.010 to 0.015 for CH_2DCCH and from 0.004 to 0.006 for CH_3CCD . Here, the predicted value for CH_2DCCH is around four times less than

the observed value (0.026), showing the importance of D-atom-transfer reactions in warm temperatures. Because CH_3CCD has yet to be observed in OMC, no comparison is made here. Deuterated allene should also form in our flow, in the same manner as deuterated propyne, however, due to its vanishing dipole moment, it is not possible to observe it in our instrument.

Doubly deuterated cyclopropenylidene; $c\text{-}C_3D_2$ is observed in nearby dark clouds and more recently doubly deuterated propyne has been discovered in the dense core L483 (Spezzano et al. 2013; Agúndez et al. 2021b). These species have a significant fractionation in these cold sources, about a few percent that of the monodeuterated species. Our results indicate that the reactions $D + C_3HD \rightarrow C_3D_2 + H$ and $D + CH_2CCD(CHDCCH) \rightarrow CH_2DCCD(CHD_2CCH) + h\nu$ can also occur in dark clouds. We looked carefully for these species in our flow but we did not see any evidence for them.

Cabezas et al. (2021b) have recently reported detection of CH_2DC_4H (but not CH_3C_4D) in TMC-1, and considered two possible routes to its formation (Cabezas et al. 2021b). One involved C_2D reaction with propyne, the other C_2H reaction with CH_2DCCH . When these reactions were assumed to proceed directly rather than with full H(D) scrambling, little deuterium enrichment in CH_2DC_4H was found. Interestingly, their alternative model invoked a D-H exchange reaction involving propyne, $D + CH_3CCH \rightarrow CH_2DCCH + H$ as part of the mechanism to account for the formation of deuterated propyne as a precursor to the observed species. Reasonable agreement with the observed fractionation for CH_2DC_4H was achieved. However, the authors assumed that the reaction was fast and barrierless, but theory and experiment both support a barrier of ~ 11 kJ mol $^{-1}$ making the reaction negligible at low temperature (Wang et al. 2000). Barriers such as this or larger are typical for H-atom reaction with closed-shell hydrocarbons, but not with radicals. Cabezas et al. (2021b) also assumed that reaction at the acetylenic site was one-third the rate at the allenic site for statistical reasons to help account for the absence of the CH_3C_4D species. We suggest analogous D/H exchange involving radicals should be considered. As mentioned above, with freeze-out conditions, the radiative association involving $D +$ propargyl brings the model closer to the observed abundances of deuterated propynes that serve as a precursor to CH_2DC_4H . Moreover, although our current ratios are still too low, a larger rate coefficient for the $D +$ propargyl reaction could reconcile model and observation. We have taken equal rates for all RA reactions involving D and H atoms, but this is not necessarily the case.

8. Astrochemical Implications

It is apparent from Figure 4 that the chemical model underestimates the deuterium fractionation of species of interest when we disregard the D-atom reactions. However, when we include the D/H exchange with radicals it improves the fractionation for $c\text{-}C_3\text{HD}$ and deuterated propynes and increases that for deuterated propargyl. In cold conditions such as TMC-1, the modeled fractionation of $c\text{-}C_3\text{HD}$ becomes 0.270, slightly higher than the observed value. For the deuterated propargyl, the fractionation increased by a factor of 1.5 and becomes close to 1% that of the fully hydrogenated species. The fractionation of $c\text{-}C_3\text{HD}$ increases to 0.334 in cold conditions with the inclusion of D-atom reactions and a freeze-out condition. In comparison to the no-D, no-freeze-out

conditions, this increases fractionation of $c\text{-C}_3\text{HD}$ by a factor of ≈ 40 . However, with this condition, the fractionation exceeds the observed value. Also, with the freeze-out on and the inclusion of D-atom reactions, the fractionation for deuterated propargyl increases by a factor of 3.5. The CH_2DCCH and CH_2CCD are now 3% and 2% of their H parent (CH_2CCH), respectively. Given the large abundance of propargyl detected in TMC-1, deuterated propargyl may be detectable in this object. According to our modeling, a significant amount of propargyl is destroyed by RA reactions, lowering their abundances. Our model predicts an increase in fractionation for deuterated propyne when we include the radiative-association reactions, but the observed abundances in TMC-1 still greatly exceed the predictions. When freeze-out is included, our calculated values increase but still fall factors of three to four below those observed. However, the analysis of the formation and destruction reactions at 1.5×10^5 yr shows that the radiative association of deuterated propargyl with H is the main formation pathway for deuterated propyne in cold conditions and we encourage further studies on this system to more accurately determine its rate coefficient. According to our calculations, the fractionation of CH_2DCCH is a factor of two to three higher than that of CH_3CCD . When the RA reactions are excluded, the fractionation ratio of $\text{CH}_2\text{DCCH}/\text{CH}_3\text{CCD}$ does not change significantly, implying that the higher fractionation for CH_2DCCH is primarily due to the greater abundance of CH_2DCCH than CH_2CCD . In warm clouds, where the fractionation by H_2D^+ species is less significant, the fractionation of hydrocarbon species also increases indicating the importance of D+ radical reactions. We find that our calculated value for the fractionation of CH_2DCCH is within a factor of two of that observed when D-atom reactions are included in our model. However, to our knowledge, the majority of the deuterated species we have focused on here do not yet have abundances reported for warm clouds such as OMC.

9. Conclusions

In this paper, chirped-pulse millimeter-wave spectroscopy in a quasi-uniform flow was used to investigate the direct D-atom incorporation to C_3H_2 and propargyl radicals at low temperature. The detection of $c\text{-C}_3\text{HD}$ shows efficient D-atom transfer to C_3H_2 radicals through D addition/H elimination. The deuterated propargyl radical, the other anticipated product, is not directly observed, although its presence is inferred from the deuterated propyne observed in the high-density region of the

flow. The formation of deuterated propyne in the flow also suggests that it can be formed in dark clouds via radiative-association reactions with H atoms. Our models also indicate that such radiative-association reactions of H and D atoms with hydrocarbon radicals can contribute significantly to deuterium fractionation. Laboratory and theoretical studies are thus needed to determine the associated rate coefficients. Concurrent to experiments, the dark cloud modeling demonstrated an increased fractionation for all deuterated species in this study, particularly when freeze-out was included. This preliminary study demonstrates that D-H exchange reactions are an important and overlooked pathway for deuterium fractionation in astrochemical environments. We encourage modelers to incorporate such reactions in models of deuterium chemistry that are more detailed in terms of both physics and chemistry than those discussed here.

This work was supported by the NSF under award No. CHE-1955239. T.J.M. thanks the STFC for support through grants ST/P000312/1 and ST/T000198/1 and gratefully acknowledges the receipt of a Leverhulme Emeritus Fellowship.

Appendix

Figure A1 shows modeled fractional abundances for all species observed in this study using TMC-1 conditions.

Table A1 provides millimeter-wave transition frequencies and associated data relevant to the species observed in this study.

Further Astrochemical Modeling Details

Table A2 Summarizes the new reactions added to the reaction network. The references for the rates are included in the table. The (*) indicates the values obtained from the corresponding non-deuterated reaction. When no experimental or theoretical data is available, the rate coefficients are estimated from corresponding high-pressure H-atom recombination reactions using reasonable assumptions based on statistical ratios (e.g., $\text{D} + \text{CH}_2\text{CCH}$, Harding et al. 2007). For these back reactions, the barrier, γ , is the difference in zero-point energy of the D and H species. However, since we calculate all models at low temperatures, once the barrier is greater than about $6T_g$, then the back reaction, i.e., the H-atom reaction, becomes unimportant and other reactions such as with ions dominate loss of the deuterated species.

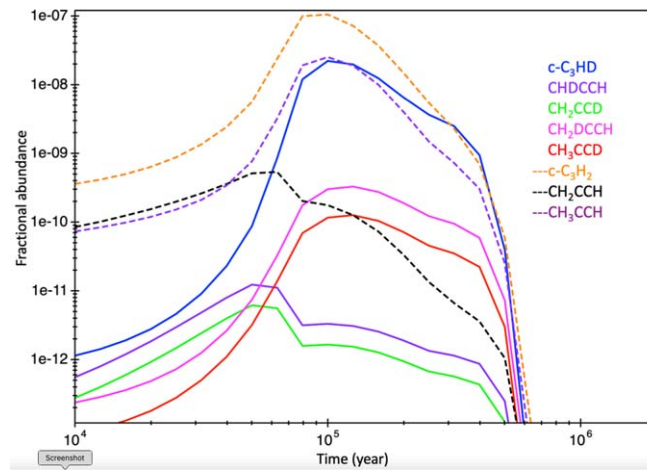


Figure A1. The fractional abundance of each species observed in this study was determined using UDfA Rate 13 codes and an updated, deuterated version of the UDfA Rate 12 network. The fractional abundance of each species is calculated using new D-atom reactions and freeze-out conditions. See main text for more details.

Table A1
Rotational Transition Frequency, Lower State Energy, Transition Quantum Numbers, and Line Strength Value of Each Species Observed in this Study

Species	Transition Frequency (GHz)	Lower State		Line Strength Value ($S\mu^2$)
		Energy (cm^{-1})	$J_{\text{up}}-J_{\text{low}}$	
CH ₃ CCD	77.880	5.19	5 ₀ -4 ₀	5.89
c-C ₃ HD	79.812	1.40	2 ₁₂ -1 ₀₁	41.58
CH ₂ DCCH	80.902	5.39	5 ₂₄ -4 ₂₃	3.07
c-C ₃ H ₂	82.966	8.38	3 ₁₂ -3 ₀₃	31.33
l-C ₃ H ₂	83.933	13.48	4 ₁₃ -3 ₁₂	189.13
CH ₃ CCH	84.457	6.14	5 ₀ -4 ₀	6.14

Table A2
The New Rates Added to the Rate File

Reaction Type	Reaction	α	β	γ	Reference
NN	D+H ₂ CCC → C ₃ HD+ H	2.00E-10	0	0	KIDA*
NN	H+C ₃ HD → H ₂ CCC + D	2.00E-10	0	575	KIDA*
NN	D + CH ₂ CCH → CHDCCH + H	6.67E-11	0	0	
NN	D + CH ₂ CCH → CH ₂ CCD + H	3.33E-11	0	0	
NN	H + CHDCCH → CH ₂ CCH + D	1.00E-10	0	892	
NN	H + CH ₂ CCD → CH ₂ CCH + D	1.00E-10	0	865	
NN	D+C ₃ H ₂ → C ₃ HD + H	4.00E-11	0	0	
NN	H+C ₃ HD → C ₃ H ₂ + D	4.00E-11	0	936	
NN	H+H ₂ CCC → C ₃ H ₂ + H	2.00E-10	0	0	KIDA
NN	D+C ₂ H → C ₂ D+H	5.00E-11	0	0	
NN	D + HCO → DCO + H	5.00E-11	0	0	
NN	H+C ₂ D → C ₂ H+D	5.00E-11	0	654	
NN	H + DCO → HCO + D	5.00E-11	0	630	
NN	D + HCCCH → C ₃ HD + H	1.00E-10	0	0	KIDA*
NN	H+C ₃ HD → HCCCH + D	1.00E-10	0	1300	KIDA*
NN	H + HCCCD → C ₃ HD + H	1.00E-10	0	0	KIDA*
NN	H+C ₃ HD → HCCCD + H	1.00E-10	0	2000	KIDA*
NN	H + HCCCH → C ₃ H ₂ + H	1.00E-10	0	0	KIDA
NN	H+C ₃ H ₂ → HCCCH + H	1.00E-10	0	2200	KIDA
NN	H + HCCCD → C ₃ H ₂ + D	1.00E-10	0	0	KIDA
NN	D+C ₃ H ₂ → HCCCD + H	1.00E-10	0	2900	KIDA*
RA	H + CH ₂ CCH → CH ₃ CCH + PHOTON	1.00E-13	-1.5	0	KIDA
RA	H + CH ₂ CCH → CH ₂ CCH ₂ + PHOTON	1.00E-13	-1.5	0	KIDA
RA	H + CHDCCH → CH ₂ DCCH + PHOTON	1.00E-13	-1.5	0	KIDA*
RA	H + CH ₂ CCD → CH ₃ CCD+ PHOTON	1.00E-13	-1.5	0	KIDA*

Table A2
(Continued)

Reaction Type	Reaction	α	β	γ	Reference
RA	D + CH ₂ CCH → CH ₂ CCHD + PHOTON	1.00E-13	-1.5	0	KIDA*
RA	D + CH ₂ CCH → CH ₃ CCD + PHOTON	3.33E-14	-1.5	0	KIDA*
RA	D + CH ₂ CCH → CH ₂ DCCH + PHOTON	6.66E-14	-1.5	0	KIDA*
RA	H + C ₃ H ₂ ⁺ → C ₃ H ₃ ⁺ + PHOTON	2.00E-15	0	0	Ref ^a
RA	D + C ₃ H ₂ ⁺ → C ₃ H ₂ D ⁺ + PHOTON	2.00E-15	0	0	Ref ^{a*}
RA	D + C ₃ H ₂ ⁺ → CH ₂ CCD ⁺ + PHOTON	6.66E-16	0	0	Ref ^a
RA	D + C ₃ H ₂ ⁺ → CHDCCH + PHOTON	1.33E-15	0	0	Ref ^{a*}
RA	H + CH ₂ CCD → CH ₂ CCHD + PHOTON	1.00E-13	-1.5	0	KIDA*
RA	H + CHDCCH → CH ₂ CCHD + PHOTON	1.00E-13	-1.5	0	KIDA*
DR	C ₃ H ₃ ⁺ + e ⁻ → H ₂ CCC + H	2.00E-08	-0.50	0	KIDA
DR	C ₃ H ₂ D ⁺ + e ⁻ → HDCCC + H	1.33E-08	-0.5	0	KIDA*
DR	C ₃ H ₂ D ⁺ + e ⁻ → H ₂ CCC + D	6.66E-09	-0.5	0	KIDA*
DR	C ₃ H ₃ ⁺ + e ⁻ → HCCCH + H	5.00E-08	-0.5	0	KIDA
DR	C ₃ H ₂ D ⁺ + e ⁻ → HCCCD + H	3.33E-08	-0.5	0	KIDA*
DR	C ₃ H ₂ D ⁺ + e ⁻ → HCCCH + D	1.67E-08	-0.5	0	KIDA*
IN	H ⁺ + CH ₃ CCH → C ₃ H ₃ ⁺ + H ₂	7.50E-10	-0.5	0	KIDA
IN	H ⁺ + CH ₃ CCH → CH ₂ CCH ⁺ + H ₂	7.50E-10	-0.5	0	KIDA
IN	H ⁺ + CH ₂ CCH ₂ → C ₃ H ₃ ⁺ + H ₂	7.50E-10	0	0	KIDA
IN	H ⁺ + CH ₂ CCH ₂ → CH ₂ CCH ⁺ + H ₂	7.50E-10	0	0	KIDA
CE	H ⁺ + CH ₂ CCH ₂ → C ₃ H ₄ ⁺ + H	1.50E-9	0	0	KIDA
IN	He ⁺ + CH ₃ CCH → C ₃ H ₃ ⁺ + He + H	2.00E-10	-0.5	0	KIDA
IN	He ⁺ + CH ₃ CCH → CH ₂ CCH ⁺ + He + H	2.00E-10	-0.5	0	KIDA
IN	He ⁺ + CH ₂ CCH ₂ → C ₃ H ₃ ⁺ + He + H	2.00E-10	0	0	KIDA
IN	He ⁺ + CH ₂ CCH ₂ → CH ₂ CCH ⁺ + He + H	2.00E-10	0	0	KIDA

Notes. The rate coefficients in this table are expressed in the standard form: $k(T) = \alpha(T/300)^\beta \exp(-\frac{\gamma}{T}) \text{ cm}^3 \text{ s}^{-1}$. All the barriers adopted ensure that the back reactions with H atoms are unimportant in setting deuterium fraction for the species considered here. NN: neutral-neutral; RA: radiative association; DR: dissociative recombination; IN: ion-neutral; CE: charge exchange.

^a (Loison et al. 2017).

ORCID iDs

Tom J Millar  <https://orcid.org/0000-0001-5178-3656>
 Arthur G. Suits  <https://orcid.org/0000-0001-5405-8361>

References

- Abeyskera, C., Joalland, B., Ariyasingha, N., et al. 2015, *JPCL*, 6, 1599
 Abeyskera, C., Zack, L. N., Park, G. B., et al. 2014, *JChPh*, 141, 214203
 Agúndez, M., Cabezas, C., Tercero, B., et al. 2021a, *A&A*, 647, L10
 Agúndez, M., Roueff, E., Cabezas, C., Cernicharo, J., & Marcelino, N. 2021b, *A&A*, 649, A171
 Agúndez, M., & Wakelam, V. 2013, *ChRv*, 113, 8710
 Albertsson, T., Semenov, D. A., Vasyunin, A. I., Henning, T., & Herbst, E. 2013, *ApJS*, 207, 27
 Amano, T. 2006, *RSPTA*, 364, 2943
 Bacmann, A., Lefloch, B., Ceccarelli, C., et al. 2003, *ApL*, 585, L55
 Bell, M. B., Avery, L. W., Matthews, H. E., et al. 1988, *ApJ*, 326, 924
 Broderick, B. M., Suas-David, N., Dias, N., & Suits, A. G. 2018, *PCCP*, 20, 5517
 Brown, P. D., & Millar, T. J. 1989a, *MNRAS*, 240, 25P
 Brown, P. D., & Millar, T. J. 1989b, *MNRAS*, 237, 661
 Brünken, S., Sipilä, O., Chambers, E. T., et al. 2014, *Natur*, 516, 219
 Cabezas, C., Endo, Y., Roueff, E., et al. 2021a, *A&A*, 646, L1
 Cabezas, C., Fuentetaja, R., Roueff, E., et al. 2022, *A&A*, 657, L5
 Caselli, P., Stantcheva, T., Shalabiea, O., Shematovich, V. I., & Herbst, E. 2002a, *P&SS*, 50, 1257
 Caselli, P. 2002b, *P&SS*, 50, 1133
 Caselli, P., Sipilä, O., & Harju, J. 2019, *RSPTA*, 377, 20180401
 Ceccarelli, C., Caselli, P., Bockelée-Morvan, D., et al. 2014, in *Protostars and Planets VI*, ed. H. Beuther et al. (Tucson, AZ: Univ. Arizona Press)
 Cernicharo, J., Cabezas, C., Agúndez, M., et al. 2021, *A&A*, 648, L3
 Chantzos, J., Spezzano, S., Caselli, P., et al. 2018, *ApJ*, 863, 126
 Chen, H.-R., Liu, S.-Y., Su, Y.-N., & Zhang, Q. 2010, *ApJL*, 713, L50
 Cox, P., Walmsley, C. M., & Güsten, R. 1989, *A&A*, 209, 382
 Crosswell, K., & Dalgarno, A. 1985, *ApJ*, 289, 618
 Dalgarno, A., & Lepp, S. 1984, *ApJL*, 287, L47
 Dias, N., Gurusinghe, R. M., & Suits, A. G. 2022, *JPCA*, 126, 5354
 Dias, N., Joalland, B., Ariyasingha, N. M., Suits, A. G., & Broderick, B. M. 2018, *JPCA*, 122, 7523
 Flower, D. R., Des Forêts, G. P., & Walmsley, C. M. 2006, *A&A*, 449, 621
 Flower, D. R., & Walmsley, C. M. 2004, *A&A*, 427, 887
 Foley, C. D., Alavi, S. T., Joalland, B., et al. 2019, *PCCP*, 21, 1528
 Gerin, M., Combes, F., Wlodarczak, G., Encrenaz, P., & Laurent, C. 1992, *A&A*, 253, L29
 Gerin, M., Wootten, H. A., Combes, F., et al. 1987, *A&A*, 173, L1
 Gurusinghe, R. M., Dias, N., Krueger, R., & Suits, A. G. 2021a, *JChPh*, 156, 014202
 Gurusinghe, R. M., Dias, N., Mebel, A. M., & Suits, A. G. 2021b, *JPCL*, 13, 91
 Harding, L. B., Klippenstein, S. J., & Georgievskii, Y. 2007, *JPCA*, 111, 3789
 Hébrard, E., Dobrijevic, M., Loison, J.-C., et al. 2013, *A&A*, 552, A132
 Herbst, E. 2003, *SSRv*, 106, 293
 Howe, D. A., & Millar, T. J. 1993, *MNRAS*, 262, 868
 Kawaguchi, K., Kaifu, N., Ohishi, M., et al. 1991, *PASJ*, 43, 607
 Klippenstein, S. J., Miller, J. A., & Jasper, A. W. 2015, *JPCA*, 119, 7780
 Lee, Y.-R., & Lin, S.-M. 1998, *JChPh*, 108, 134
 Lis, D., Roueff, E., Gerin, M., et al. 2002, *ApL*, 571, L55
 Loison, J.-C., Agúndez, M., Wakelam, V., et al. 2017, *MNRAS*, 470, 4075
 Loomis, R. A., Burkhardt, A. M., Shingledecker, C. N., et al. 2021, *NatAs*, 5, 188
 Majumdar, L., Gratier, P., Ruaud, M., et al. 2016, *MNRAS*, 466, 4470
 Margitan, J. J., Kaufman, F., & Anderson, J. G. 1975, *CPL*, 34, 485
 Markwick, A. J., Charnley, S. B., Butner, H. M., & Millar, T. J. 2005, *ApL*, 627, L117
 Markwick, A. J., Charnley, S. B., & Millar, T. J. 2001, *A&A*, 376, 1054
 McElroy, D., Walsh, C., Markwick, A. J., et al. 2013, *A&A*, 550, A36
 Miettinen, O., Hennemann, M., & Linz, H. 2011, *A&A*, 534, A134
 Millar, T. J. 1997, *SymIAU*, 178, 75
 Millar, T. J., Bennett, A., & Herbst, E. 1989, *ApJ*, 340, 906
 Nakajima, A., Fuke, K., Tsukamoto, K., Yoshida, Y., & Kaya, K. 1991, *JPhCh*, 95, 571
 Oldham, J. M., Abeyskera, C., Baptiste, J., et al. 2014, *JChPh*, 141, 154202
 Parise, B., Castets, A., Herbst, E., et al. 2004, *A&A*, 416, 159
 Parise, B., Ceccarelli, C., Tielens, A., et al. 2006, *A&A*, 453, 949

- Parise, B., Ceccarelli, C., Tielens, A., et al. 2002, *A&A*, 393, L49
- Parise, B., Du, F., Liu, F. C., et al. 2012, *A&A*, 542, L5
- Park, G. B., & Field, R. W. 2016, *JChPh*, 144, 200901
- Punanova, A., Caselli, P., Pon, A., Belloche, A., & André, P. 2016, *A&A*, 587, A118
- Roberts, H., Herbst, E., & Millar, T. J. 2002, *MNRAS*, 336, 283
- Roberts, H., Herbst, E., & Millar, T. J. 2003, *ApL*, 591, L41
- Roberts, H., & Millar, T. J. 2000, *A&A*, 361, 388
- Roberts, H., & Millar, T. J. 2007, *A&A*, 471, 849
- Roueff, E., & Gerin, M. 2003, *SSRv*, 106, 61
- Roueff, E., Lis, D. C., Van der Tak, F. F. S., Gerin, M., & Goldsmith, P. F. 2005, *A&A*, 438, 585
- Solomon, P. M., & Woolf, N. J. 1973, *ApJL*, 180, L89
- Spezzano, S., Brünken, S., Schilke, P., et al. 2013, *ApL*, 769, L19
- Spezzano, S., Gupta, H., Brünken, S., et al. 2016, *A&A*, 586, A110
- Sutton, E. C., Peng, R., Danchi, W. C., et al. 1995, *ApJS*, 97, 455
- Tercero, B., Vincent, L., Cernicharo, J., Viti, S., & Marcelino, N. 2011, *A&A*, 528, A26
- Tiné, S., Roueff, E., Falgarone, E., Gerin, M., & Pineau des Forêts, G. 2000, *A&A*, 356, 1039
- Turner, B. E. 2001, *ApJS*, 136, 579
- Van der Tak, F. F. S., Schilke, P., Müller, H. S. P., et al. 2002, *A&A*, 388, L53
- Vastel, C., Phillips, T. G., Ceccarelli, C., & Pearson, J. 2003, *ApL*, 593, L97
- Wakelam, V., Dartois, E., Chabot, M., et al. 2021, *A&A*, 652, A63
- Wakelam, V., Herbst, E., Loison, J. C., et al. 2012, *ApJS*, 199, 21
- Walmsley, C. M., & Flower, D. R. 2004, *A&A*, 418, 1035
- Wang, B., Hou, H., & Gu, Y. 2000, *JChPh*, 112, 8458
- Watson, W. D. 1977, *CNO Isotopes in Astrophysics* (Berlin: Springer), 105
- Willacy, K., & Millar, T. J. 1998, *MNRAS*, 298, 562